Malaysian Journal of Chemistry, 2025, Vol. 27(3), 261-271
(Special Issue: *2nd International Science and Technology Colloquium, i-COSTECH 2024*)

Structural Analysis of 5,7-dihydroxy-3-flavene Binding in *Canavalia ensiformis* Urease Active Site via GFN2-xTB Quantum Mechanical Method

Lee Sin Ang[1], Zaidi Ab Ghani[1], Shukor Sanim Mohd Fauzi[2], Norlin Shuhaime[1], Sharifah Zati Hanani Syed Zuber[3] and Mohd Hafiz Yaakob[1]*

[1]Faculty of Applied Sciences, Universiti Teknologi MARA Perlis Branch, Arau Campus, 02600 Arau, Perlis, Malaysia

[2]College of Computing, Informatics and Mathematics, Universiti Teknologi MARA Perlis Branch, Arau Campus, 02600 Arau, Perlis, Malaysia

[3]Faculty of Chemical Engineering and Technology, Kompleks Pusat Pengajian Jejawi 3, Kawasan Perindustrian Jejawi, Universiti Malaysia Perlis, 02600 Arau, Perlis, Malaysia

*Corresponding author (e-mail: hafiz959@uitm.edu.my)

Urease is an enzyme that is crucial for the hydrolysis of urea, a process that can have a significant impact on the environment when in excess. There is growing interest in identifying natural compounds that can inhibit urease activity. Flavonoids, a category of phytochemicals found in plants, have shown significant potential as urease inhibitors. Studies suggest that certain flavonoids such as 5,7-dihydroxy-3-flavene (abbreviated as D2FLA) demonstrate significant urease inhibition, exceeding the effectiveness of various natural, synthetic and metal-based urease inhibitors. To elucidate the molecular basis of this inhibition and determine the optimal binding configurations, we performed quantum mechanical GFN2-xTB calculations, mainly studying the interaction of D2FLA with the urease active site in different spatial arrangements. The optimal binding position of D2FLA at the active site of the urease was determined to be at position 3, which corresponds to an interaction energy of −56.03 kcal mol^{-1}. Topological analysis showed the absence of typical covalent bonds between the interacting atoms; Only weak interactions were observed. The hydroxyl groups, which have the most significant negative local potential in ring A of the flavonoids, predominantly facilitate noncovalent and metal acceptor interactions with the nickel center and residues of the urease, indicating their possible involvement in the inhibitory activity of the flavonoids toward the urease enzyme.

Keywords: Urease; flavonoids; inhibitor; GFN2-xTB; semiempirical

Received: September 2024; Accepted: December 2024

Nitrogen fertilizers are the most used nutrients in agriculture. In 2021 to 2022, global nitrogen fertilizer consumption exceeded 109 million tons, with forecasts predicting a four- to five-fold increase by 2050 [1]. Urea plays a central role in this expansion, accounting for around 57% of these fertilizers [2, 3]. Once urea is applied to the soil, it undergoes hydrolysis, a reaction catalyzed by the urease enzyme. Urease, a nickel-dependent metalloenzyme, accelerates the breakdown of urea into ammonia (NH_3) and carbon dioxide (CO_2). This reaction occurs quickly and results in a rapid release of NH_3, which can volatilize and escape into the atmosphere. The resulting NH_3 losses not only reduce the efficiency of fertilizer use, but also have a negative impact on crop yields and the environment, as plants have a limited ability to absorb excess nutrients [4]. Previous research indicates that when urease is present, the rate of the hydrolysis reaction is more than 10^{14} times faster than when the reaction is not catalyzed [5, 6].

To mitigate the environmental impact of urease activity and promote sustainable agricultural practices, effective strategies are essential. The rapid breakdown of urea by urease results in significant NH_3 losses, which contribute to soil degradation, air pollution and reduced fertilizer efficiency [7-10]. Therefore, inhibiting or lowering the activity of urease enzyme is a crucial step in minimizing these adverse effects. Although traditional synthetic urease inhibitors such as NBPT and hydroquinone are effective and often exhibit low half-maximal inhibitory concentration (IC_{50}) values, they often pose environmental and health risks due to their chemical resistance and potential toxicity [11, 12]. In contrast, natural inhibitors such as flavonoids have proven to be a promising alternative. Flavonoids, a diverse class of natural compounds found in plants, offer the advantages of being biodegradable, less toxic, and environmentally friendly. Their ability to interact with the active site of the urease enzyme

†Paper presented at the 2nd International Science and Technology Colloquium (i-COSTECH 2024)

has gained renewed attention as a sustainable solution for urease inhibition [13-17]. This makes it an attractive research focus and meets the growing demand for environmentally friendly agricultural practices.

Investigating the complex interactions within the active site of urease, with its numerous binding sites, presents significant challenges for computational methods. While Density Functional Theory (DFT) is often favoured for its accuracy in predicting electronic structures and reaction mechanisms, it is computationally prohibitive for large systems such as urease-enzyme complexes. The development of the GFN2-xTB method has addressed this limitation by providing a semi-empirical quantum mechanical approach that significantly reduces computational costs while maintaining reliable accuracy. Unlike DFT, GFN2-xTB is optimized for large biological systems and enables efficient simulations of transition metal complexes, non-covalent interactions, and protein structures [18, 19]. This method has proven effective in predicting binding energies and structural parameters in enzyme-inhibitor complexes, making it a practical and powerful tool for studying urease-flavonoid interactions. By balancing computational efficiency with accuracy, GFN2-xTB offers a valuable alternative to more resource-intensive methods, particularly in the context of large-scale biological studies.

This study focuses on the binding mode of 5,7-dihydroxy-3-flavene in various spatial arrangements within the urease active site. By employing the GFN2-xTB method, this research aims to provide valuable structural and electronic insights into the interaction between urease and flavonoids, contributing to the development of effective urease inhibitors for sustainable agriculture.

COMPUTATIONAL DETAILS

Urease Active Site Structure

The high ureolytic activity of *Canavalia ensiformis* urease, also known as jack bean urease, led to its selection in this study. According to reports, depending on the state of the enzyme, the urease could display ureolytic activity as high as 2700–3500 μmol urea/min mg [20]. The 3LA4 *Canavalia ensiformis* crystal structure from RCSB Protein Data Bank was selected to be used in this study due to its appropriate experiment method (x-ray diffraction), resolution (2.05 Å), R-value work (0.183) and R-value free (0.201) data [21,22]. It was reported that the active site of the enzyme, which contains dinickel metals, is where the catalytic activity of the enzyme occurs. Therefore, the residues His407, His409, Lys490, His492, Asp494, His519, His545, Cys592, His593, Arg609, Asp633, and Ala636 were retained when the 3LA4 crystal structure was truncated to the active site. It was reported that the enzyme's catalytic activity takes place in the active site where dinickel metals are located [22-24]. 239 atoms and 1152 electrons were presented in the modified urease active site model (**Figure 1**).

Flavonoids Structure

For the flavonoids inhibitor structure, 5,7-dihydroxy-3-flavene (denoted as D2FLA) (**Figure 1**) was selected due to its low half maximal inhibitory concentration value (IC_{50} = 33.20 ± 1.80 μM) [17]. The backbone structure of 3-flavene was retrieved from the Cambridge Structural Database (CSD) (CID:1805918) and modified into D2FLA using GaussView software (version 5.0). 30 atoms and 126 electrons were presented in the D2FLA model.

Semiempirical Tight Binding Calculations and Analysis

The binding between the urease active site and D2FLA was processed using PyRx 0.8, a virtual screening tool to determine the preferred orientation of D2FLA in the vicinity of the urease active site. Five structural complexes (labelled as P1 to P5) with lowest binding energy were selected and checked using GaussView software to correct any improper issues with the structures before subjecting them to the quantum mechanical calculation. Geometry optimization of all complexes was performed by GFN2-xTB method, a semiempirical quantum approach implemented in the xTB software (version 6.6.1). All calculations are set to default set up and values. All atoms in the system were fixed except for two nickel ions, the bridging hydroxide ions between two nickel and the D2FLA molecule. The atoms were fixed to help simulate the effect of the environment of the urease enzyme without fully including it in the quantum mechanical calculation. For comparison purpose, the performance of GFN2-xTB method was compared to the DFT method of B3LYP/6-31G**. The interaction strength between the binding between urease active site and D2FLA for all conformations was calculated by Equation (1):

$$E^{\text{int}} = E_{\text{urease+D2FLA}} + E_{\text{urease}} + E_{\text{D2FLA}} \quad (1)$$

For the first column (Geometry from PyRx, GFN2-xTB), the energies were calculated using initial geometry of complexes from docking results with no optimization settings applied, by GFN2-xTB method. However, for the second column (Optimized geometry by GFN2-xTB), both optimization and energy calculation were done by the GFN2-xTB method. For the third column (Optimized geometry by B3LYP/6-31G**), the geometry of the optimized complexes from the second column, were submitted to DFT calculations to benchmark the range of energies calculated between both methods.

Electrostatic potential (ESP) and quantum theory of atoms in molecules (QTAIM) analysis of the optimized complexes were performed by Multiwfn software [25]. The ESP coloured molecular surface map was rendered by VMD molecular graphics viewer (version 1.9.4) based on the outputs of Multiwfn. The grid spacings were set to 0.2 Bohr and the isosurface of the vdW surface was 0.001 e/bohr^3 [26]. In QTAIM analysis, bond critical points (3,–1) and the associated topological and energetic properties such as Laplacian of electron density, Lagrangian kinetic energy, potential energy density and hydrogen bond binding energy ($BE_{H\text{-}bond}$) were calculated to evaluate the nature of bonding interactions [27,28]. Theoretical bond degree parameter ($BD = H_b/\rho_b$) as a function of $|V_b|/G_b$ plot for the strongest and lowest interaction were analyzed to identify key features of the electron density distribution that characterize the bonding and non-covalent interactions involved in the system. The interatomic interactions were divided into three types: *pure* closed shell (CS, region I, $\nabla^2\rho_b > 0$, $H_b > 0$), *transit* closed shell (CS, region II, $\nabla^2\rho_b > 0$, $H_b < 0$), and *pure* shared shell (SS, region III, $\nabla^2\rho_b < 0$, $H_b < 0$). The $BE_{H\text{-}bond}$ for the selected bond critical points (BCPs) were calculated by Equation (2):

$$BE_{H\text{-}bond} = -332.34 \times \rho_{BCP}/\text{a.u.} - 1.0661 \qquad (2)$$

RESULTS AND DISCUSSION

Geometry Optimization and Interaction Energy Analysis

Based on frequency calculations, all computational work confirmed that there was no imaginary modes, meaning that no unoptimized or transition state complexes were included in the analysis. The urease-D2FLA complexes fit well with the GFN2-xTB approach as they preserve the good geometry of the local atomic environments and ensure accurate structural representation without damaging the structure.

The binding mode between urease active site and D2FLA are depicted in **Table 1**. It was discovered through the configuration analysis of the optimized geometries that the D2FLA structure exhibits nearly identical trends in how it approaches binding to the urease active site's centre. Ring A of D2FLA was observed to be oriented and closer to the nickel and hydroxide ions of the active site. This finding is expected, since ring A contains two hydroxyl groups at carbon 5 and 7. The hydroxyl groups have tendency to chelate with metal ions and its nearby residues [29]. This prevents the enzyme from binding to its natural substrate (urea) and inhibits the catalytic activity of the enzyme by blocking the necessary interaction between the nickel ions and the urea. Therefore, the presence of flavonoids also triggered conformational changes in the active site of the enzyme, potentially altering the structure of the enzyme [30,31]. This could reduce the activity of the enzyme due to misalignment of the catalytic residues, even if the substrate can bind.

The interaction energies for all complexes are listed in **Table 2**. Between all positions, the P3 position exhibits the strongest interaction energy between urease and D2FLA, with an interaction energy calculated as –56.03 kcal mol^{-1}, indicating a strong attraction between the urease and D2FLA.

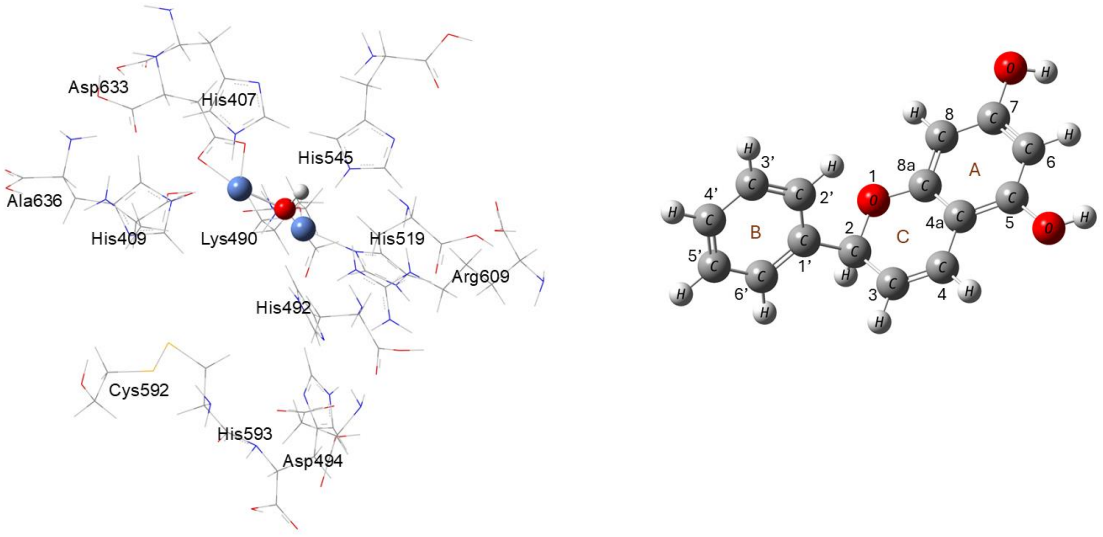

Figure 1. (*Left*) Structure of the urease active site from *Canavalia ensiformis*. Blue spheres represent nickel ions, red and white spheres represent a hydroxide ion, and the wireframe indicates urease residues. (*Right*) Structure of D2FLA.

Table 1. Initial and final geometry of urease-D2FLA complexes at various positions. The molecule in wireframe is the residues of urease including the hydroxide ion, and the molecule in tube is D2FLA. Nickel ions are represented in blue spheres. For the sake of clarity, hydrogen atoms have been omitted.

Position	Initial geometry (from PyRx)	Final geometry (optimized by GFN2-xTB)
P1	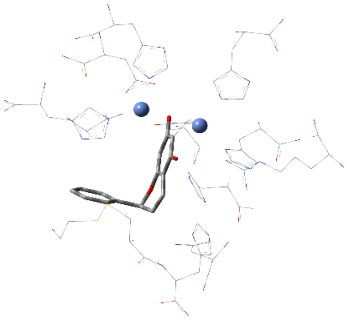	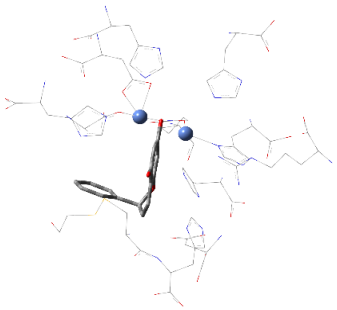
P2	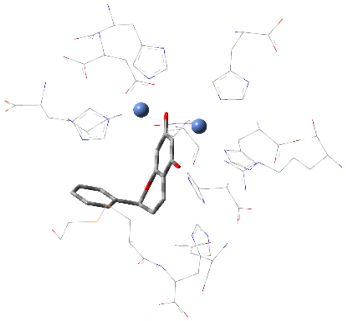	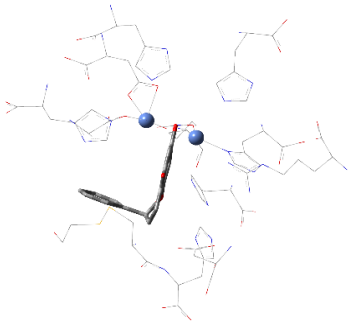
P3	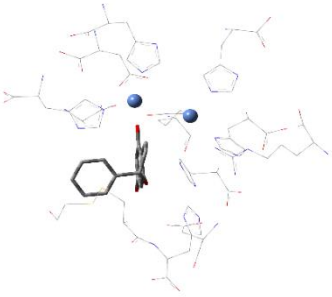	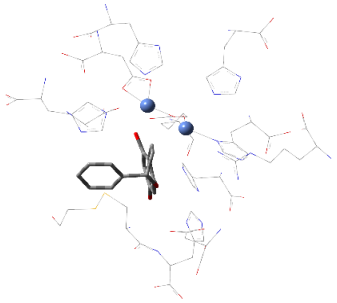
P4	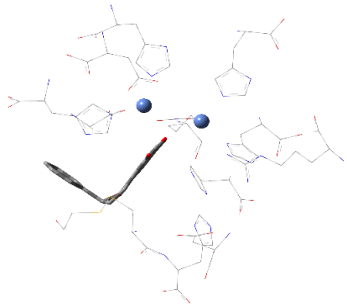	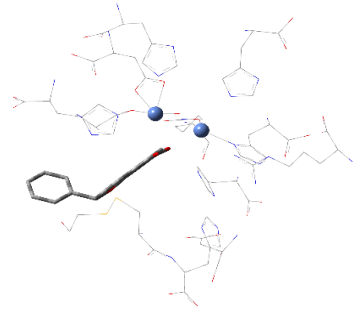
P5	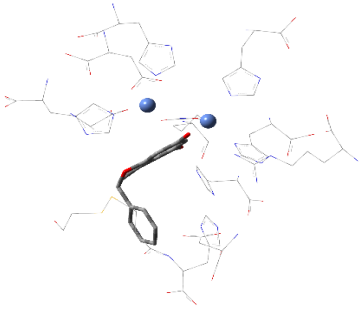	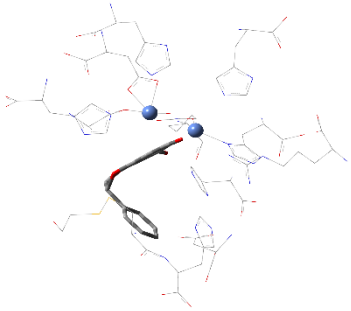

Table 2. Interaction energies (E^{int}) for urease-D2FLA complexes by GFN2-xTB and B3LYP/6-31G** method.

Position	Interaction energy, E^{int} (kcal mol^{-1})		
	Geometry from PyRx, GFN2-xTB	Optimized geometry by GFN2-xTB	Optimized geometry by B3LYP/6-31G**
P1	–6.86	–44.92	–49.87
P2	–3.34	–37.12	–47.95
P3	–10.32	–56.03	–57.82
P4	–2.27	–53.86	–53.04
P5	–7.80	–51.65	–48.99

This strong interaction is likely facilitated by the strategic positioning of both hydroxyl groups on ring A, which form strong attraction with the nickel centre in the urease active site, leading to a more stable complex. In contrast, the least favourable interaction is observed at the P2 position, with an interaction energy of –37.12 kcal mol^{-1}. The weaker interaction at this position can be attributed to the orientation of the hydroxyl group on carbon 5, which is directed towards an empty space away from the nickel centre and other critical residues in the urease active site, reducing its contribution to binding stability. The close agreement of the results with the literature suggested that, the positioning and orientation of hydroxyl groups significantly influence the binding affinity between molecules [32,33]. This suggests that the geometry of interaction plays a crucial role in determining the strength of binding between flavonoids and urease, highlighting the importance of considering both electronic and spatial factors in designing potent urease inhibitors. The energies calculated from the geometry generated by PyRx tend to be lower than those from the GFN2-xTB and DFT method. This may be due to the PyRx method that did not optimize the structure of the complexes to the optimum level, revealing that some parts of the interactions were not captured and need to be supported by proper quantum mechanical approach [34].

Variations in atomic distances greatly influence the interaction energy between atoms or molecules, thereby affecting the nature of chemical bonding. Typically, shorter atomic distances result in stronger interactions, such as covalent or ionic bonds, while longer distances are associated with weaker interactions like van der Waals forces or other noncovalent interactions. These distance-related variations also impact the stability and reactivity of complexes, which in turn plays a critical role in the effectiveness of flavonoids as urease inhibitors. The changes of key interatomic distances between nickel ions, hydroxyl group in D2FLA, and hydroxide ion of the strongest and weakest urease-D2FLA interaction energy are shown in **Table 3**. The purpose of **Figure 2** is to enhance and make it easier to understand the interatomic distances displayed in **Table 3**. In this study, the Ni-Ni distance generated from GFN2-xTB method was observed between 3.66 to 3.67 Å. The value agrees with the Ni-Ni distances from 3.26 to 3.7 Å that have been reported in earlier research using a variety of computational and experimental techniques [23, 35, 36]. The close agreement between our results and these values underscores the accuracy and reliability of the GFN2-xTB method in modelling the nickel centre of urease.

In addition to the Ni-Ni distance, other interatomic distances within the urease active site must be considered to gain a comprehensive understanding of the enzyme's functionality and inhibition mechanism. Specifically, in the urease-D2FLA complex, an increase in interaction energy was observed as the A ring of D2FLA approached the Ni_1 and Ni_2 ion. The GFN2-xTB calculations show that the Ni_1-O_5 and Ni_2-O_7 interatomic distances were shorter than those at the other positions, which were 3.56 Å and 5.18 Å, respectively. The P5 position also has the same Ni_1-O_5 distance as P3, but the Ni_2-O_7 was quite distant away. This observation suggests that the closer proximity of the A ring to Ni_1 may enhance the binding affinity of D2FLA to the urease enzyme, potentially through stronger interaction with the Ni_1 and Ni_2 ion.

ESP Analysis

Electrostatic analysis plays a crucial role in predicting intermolecular interactions between the inhibitors and the urease enzyme. The chemically active centres and the atoms' reactivity are shown visually by ESP. The interaction between inhibitors and these metal ions is often mediated by electrostatic forces, which can significantly influence the binding affinity and potency of the inhibitors [37-39]. Studying the ESP of D2FLA may be helpful for a better understanding of the important interaction between flavonoids and the urease enzyme.

Table 3. Key interatomic distances (in angstrom unit, Å) between nickel ions, hydroxide ion and hydroxyl groups of D2FLA in the urease-D2FLA complexes.

Position	Interatomic distances, *r* (Å)						
	Ni_1-Ni_2	Ni_1-O_5	Ni_1-O_7	Ni_2-O_5	Ni_2-O_7	H_5-O_1	H_7-O_1
P1	3.67(3.68)	8.26(5.56)	4.67(2.14)	6.29(6.52)	2.30(2.19)	7.47(7.12)	3.84(2.33)
P2	3.66(3.67)	7.78(5.58)	3.92(2.13)	6.23(6.50)	2.32(2.19)	7.33(6.33)	3.63(1.72)
P3	3.67(3.68)	2.56(3.69)	5.18(6.14)	2.04(2.50)	6.47(6.12)	2.91(2.70)	6.70(6.26)
P4	3.67(3.68)	5.77(6.25)	2.33(2.52)	3.61(6.19)	3.24(2.64)	5.64(6.56)	2.68(1.90)
P5	3.67(3.67)	2.46(2.41)	5.58(5.64)	3.11(3.53)	4.06(6.57)	2.77(3.38)	5.70(6.04)

*The values in the brackets are before the optimization.

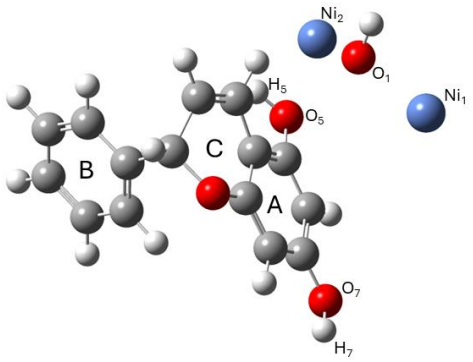

Figure 2. Close-up and labelled of D2FLA structure with nickel and bridging hydroxide of the *Canavalia ensiformis* urease active site. The image was truncated from the optimized structure at position P3 in Table 1.

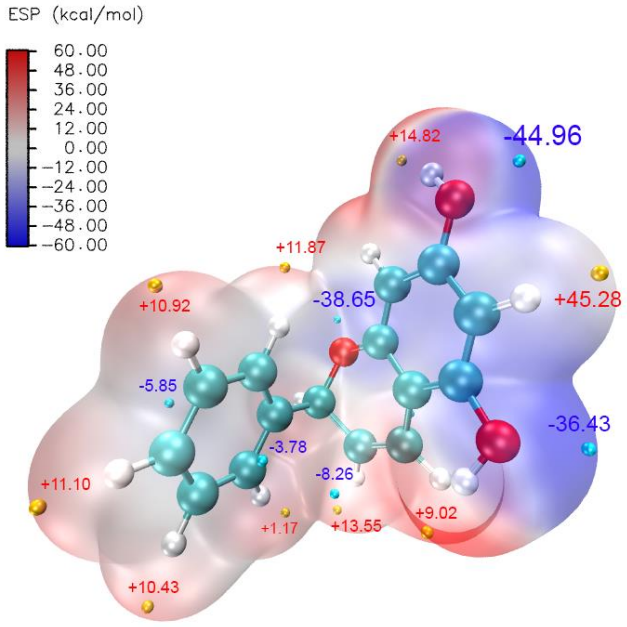

Figure 3. ESP-mapped molecular vdW surface of D2FLA. Surface local minima and maxima of ESP are represented as small blue and yellow spheres, respectively.

The ESP-mapped vdW surface along with the surface extrema of D2FLA is shown in **Figure 3**. Lone pair of oxygen atom (from the hydroxyl group) on carbon 7 of D2FLA results in the most negative ESP point on the vdW surface with a value of –44.96 kcal/mol, which is also the global minimum of D2FLA. This global minimum point contributed to the stronger interaction between the hydroxyl group and nickel centre, supported by the interatomic distance results, as shown in **Table 3**, which indicate that the most favourable complex exhibits a short interatomic distance at oxygen atom of carbon 7. This suggests that strong electrostatic attraction, coupled with the reduced interatomic distance, contributes to the stability and orientation of the complex. In addition, another significant ESP value is present in ring A, which comes from the hydroxyl group on carbon 5 and has a value of –36.43 kcal/mol. Due to these highly negative ESP values in the D2FLA structure, this region strongly interacts with the nickel centre, causing ring A to orient towards it as proved in the optimized geometry. This result aligns with observations made by other researchers, who also noted similar interactions in their studies, further supporting the significance of these electrostatic potential values in determining the orientation of ring A towards the nickel centre [14, 17]. The global maximum arising from the positively charged area located at hydrogen atom of carbon 6, and the value at this point is much larger (+45.28 kcal/mol) than others due to the presence of neighbouring oxygen atoms, which attracted a great deal of electrons from hydrogen at carbon 6.

Table 4. Selected topological parameters for urease-D2FLA at position P2 and P3, generated by Multiwfn software from the optimized structure using GFN2-xTB theoretical method.

Interatomic BCPs	$d_{A\text{-}B}$ (Å)[a]	ρ_b (e/Å^3)[b]	$\nabla^2\rho_b$ (e/Å^5)[c]	G_b/ρ_b (h e^{-1})[d]	H_b/ρ_b (h e^{-1})[e]	$\lvert V_b\rvert/G_b$[f]
D2FLA:P2						
177N-100Ni	2.114	0.550	10.852	1.479	-830.478	1.137
100Ni-77O	2.040	0.641	13.071	1.568	-700.611	1.170
27O-31Ni	2.315	0.322	7.511	1.517	155.076	0.961
146O-31Ni	2.118	0.392	10.694	1.866	-369.370	1.075
31Ni-134O	2.044	0.648	12.621	1.511	-688.382	1.173
31Ni-135O	2.316	0.341	8.019	1.546	141.077	0.965
252O-18H	3.502	0.002	0.055	1.233	1607.650	0.504
266O-1H	5.509	0.000	0.001	1.337	2219.073	0.368
203O-14H	2.981	0.008	0.205	1.164	1549.988	0.493
260H-26O	3.104	0.007	0.183	1.207	1557.772	0.509
13O-156H	3.980	0.001	0.019	1.468	2104.433	0.454
28H-147O	3.939	0.004	0.073	0.797	1066.202	0.490
23H-73O	2.320	0.074	1.371	0.987	835.728	0.677
D2FLA:P3						
149N-74Ni	2.174	0.496	9.802	1.437	-353.887	1.093
74Ni-98O	1.996	0.698	13.993	1.589	-893.492	1.214
26O-40Ni	2.040	0.581	12.930	1.664	-657.963	1.150
186O-40Ni	2.727	0.111	2.395	1.226	717.050	0.777
40Ni-161O	1.980	0.703	13.628	1.553	-958.284	1.234
40Ni-164O	1.943	0.812	14.529	1.515	-1133.867	1.284
203O-30H	1.576	0.359	4.756	0.923	1107.154	0.994
H29-186O	2.117	0.092	1.681	1.034	642.900	0.763
231S-8C	3.478	0.019	0.420	1.048	1311.581	0.523
27O-136C	2.974	0.029	0.823	1.368	1589.469	0.557
183H-26O	2.098	0.140	2.153	0.971	275.328	0.892
18H-187O	4.058	0.002	0.043	0.881	1165.534	0.496
8C-187O	3.803	0.004	0.094	1.172	1492.046	0.515

[a] Interatomic length, [b] Electron density at the BCP, [c] Laplacian of the electron density at the BCP, [d] Lagrangian kinetic energy density ratio at BCP, [e] Total energy density ratio at the BCP, [f] V_b is the potential energy density.

QTAIM Analysis

In this study, we use QTAIM analysis to investigate the topological properties of electron density within the urease-D2FLA system. The bond critical points (BCPs) generated from the analysis provide insight into the bonding characteristics, electron density distribution, and the strength of interactions that control inhibition. The QTAIM analysis revealed around 326 and 328 BCPs in each system. However, only BCPs that were associated with the Ni ions and D2FLA atoms were used for analysis because the focus is on explaining the specific interaction between urease and D2FLA. Hence, these BCPs suggest a strong interaction contributing to the inhibitory activity. For this analysis, the selected topological properties from P2 (the lowest E^{int}) and P3 (the highest E^{int}) position are gathered in **Table 4**.

In the analysis, all BCPs were identified and satisfied through Poincarè-Hopf relationship checking. For both P2 and P3 position, 13 BCPs are associated with Ni ions, D2FLA, related residues with ρ_b value between 0.002 to 0.812 e/Å^3 with the characteristics of "closed-shell" interactions (positive Laplacian; $\nabla^2\rho_b > 0$). Hence, there is no formation of pure covalent or polar-covalent from the interaction between D2FLA and urease, according to the classification of interatomic interaction analysis reported by Espinosa *et al*. [40] and Bianchi *et al*. [27]. Although the formation of a pure covalent bond between flavonoids and urease complexes is theoretically possible, there is currently no scientific evidence to support this occurrence. This observation is consistent with the research of Awllia *et al*. [41] and Kataria and Khatkar [42]. This shows that no covalent compounds are involved in the way flavonoids inactivate urease.

For the interaction between flavonoids and Ni ions for both P2 (purple triangle) and P3 (green circle) as shown in Figure 4, most of the BCPs were observed within *transit* closed shell region (region II). This indicates that the BCPs exhibits properties of both weakly shared and purely closed-shell interactions, typical of ionic interactions. However, the BCPs of P3 shows stronger covalence degree (CD) points, indicates that the flavonoids at P3 position have stronger interaction with Ni ions compared to P2 position. For the interaction between flavonoids and urease residues, the BCPs of P2 and P3 were observed within the *pure* closed shell region (region I). This suggest that these interactions are dominated by electrostatic forces, which are characteristic of non-covalent interactions like hydrogen bonds and van der Waals interactions. In this region, P3 shows a stronger interaction than P2, which is observed at points with lower softening degree (SD), indicating a stronger interaction between D2FLA and the residues at the specific points.

The identification of selected BCPs of the P2 and P3 position within the region I suggest that these critical points correspond to hydrogen bonds between D2FLA and urease residues as shown in **Table 5**.

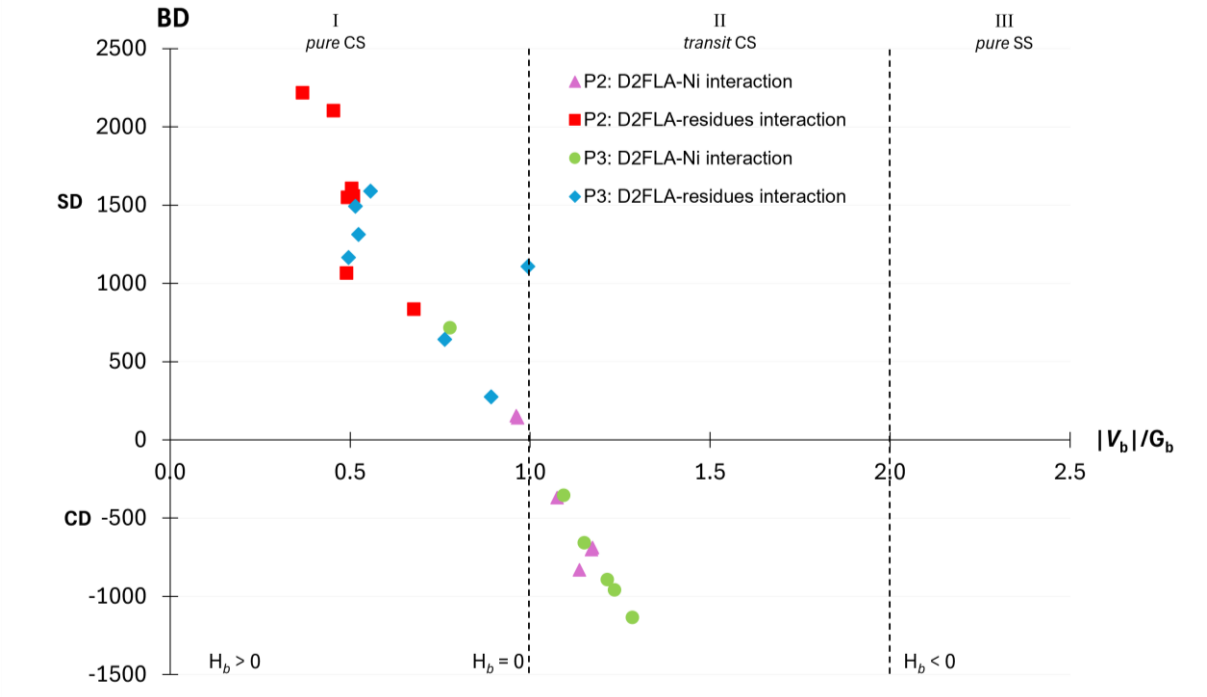

Figure 4. Selected bond degree (BD = H_b/ρ_b) as a function of $|V_b|/G_b$ plot of P2 and P3 complexes optimized by GFN2-xTB method.

Table 5. Hydrogen bond analysis of selected BCPs for the studied complexes.

Position of D2FLA	Interacting atoms X-H···Y	Urease residues involved	H-bond distance H···Y (Å)	X-H···Y angle (°)	Density of all electrons, ρ_b (e/Å^3)	$BE_{H\text{-}bond}$ (kcal mol^{-1})
P2	15C-18H···252O	Arg609	3.50	131.05	0.0003	-1.17
	2C-1H···266O	Arg609	5.50	136.35	0.0000	-1.07
	11C-14H···203O	Asp494	2.98	154.81	0.0012	-1.47
	254C-260H···26O	Arg609	3.10	117.36	0.0011	-1.42
	152C-156H···13O	His519	3.98	113.18	0.0001	-1.10
	25C-28H···147O	His519	3.94	96.92	0.0006	-1.27
P3	27O-30H···203O	Asp494	1.58	167.71	0.0531	-18.72
	26O-29H···186O	Ala636	2.18	156.43	0.0136	-5.60
	180C-183H···26O	Ala636	2.10	172.61	0.0208	-7.97

However, some of the BCPs on P2 exhibit low electron density and bond angle, below the typical range expected for hydrogen bonds, which typically have electron densities between 0.002 and 0.004 e/Å^3 and bond angles close to 180° for strong and around 120° for weaker hydrogen bonds. This low value suggests that the BCPs analyzed in P2 are likely weak and do not exhibit hydrogen bonding characteristics. This suggests that the interaction at these sites is weak, with hydrogen bond binding energies ($BE_{H\text{-}bond}$) between -1.0 and -1.5 kcal mol^{-1}, possibly a van der Waals interaction. This weak interaction corresponds to a lower E^{int}, contributing minimally to the overall stabilization of the D2FLA-urease complex. The BCPs observed at P3, which were identified between D2FLA, Asp494 and Ala636 of the urease active site, have significantly higher electron density compared to P2. This indicates the presence of a strong and medium hydrogen bond interaction between D2FLA and Asp464 and Ala636 residues. The strongest hydrogen bond in the P3 position is between the Asp494 residue and has a binding energy of -18.72 kcal mol^{-1}. These strong and medium hydrogen bond likely play a key role in maintaining the stability of the flavonoids-urease complex and may be a crucial factor in the inhibitory mechanism.

CONCLUSION

This study demonstrated that the binding conformation of 5,7-dihydroxy-3-flavene in the urease active site of *Canavalia ensiformis* is strongly influenced by the position and orientation of its hydroxyl groups. Among the different positions analyzed, the P3 position had the strongest interaction energy, calculated to be -56.03 kcal mol^{-1}, due to the strategic positioning of the hydroxyl groups on ring A, which form strong attractive forces within the nickel center in the active site of the urease. This resulted in an extremely stable complex. In contrast, the P2 position had the weakest interaction energy at -37.12 kcal mol^{-1}, which was due to the less favourable orientation of the hydroxyl groups, which did not contribute effectively to the binding stability.

Analysis of bond critical points (BCPs) also revealed that hydrogen bonds play a key role in the interaction between flavonoids and urease. Strong and medium hydrogen bonds were identified at the P3 position, particularly at residues Asp494 and Ala636, contributing to greater complex stability. In contrast, the BCPs at the P2 position showed weaker van der Waals interactions, which contributed minimally to stabilization. These results highlight the importance of both electronic and spatial factors in determining the binding strength of flavonoids to urease. Furthermore, the results highlight the need to use quantum mechanical methods such as GFN2-xTB for interaction energy predictions, as simpler approaches may not fully capture the complexity of these interactions. Future research could explore further optimization of molecular geometry and evaluate different flavonoids derivatives to develop more effective urease inhibitors.

ACKNOWLEDGEMENTS

This work was funded by the Ministry of Higher Education (MoHE) Malaysia (Fundamental Research Grant Scheme, project code: FRGS/1/2024/STG04/UITM/02/6). Most appreciate to Universiti Teknologi MARA Perlis Branch and Arau Science, Technical and Research Network (ASTeRN) research interest group for the facilities provided.

REFERENCES

1. Javed, T., Indu, I., Singhal, R. K., Shabbir, R., Shah, A. N., Kumar, P., Jinger, D., Dharmappa, P. M., Shad, M. A., Saha, D., Anuragi, H., Adamski, R. and Siuta, D. (2022) Recent advances in agronomic and physio-molecular approaches for improving nitrogen use efficiency in crop plants. *Frontiers in Plant Science*, **13**, 877544.

2. Chataut, G., Bhatta, B., Joshi, D., Subedi, K. and Kafle, K. (2023) Greenhouse gases emission from agricultural soil: A review. *Journal of Agriculture and Food Research*, **11**, 100533.

3. Nadarajan, S. and Sukumaran, S. (2021) Chapter 12 - Chemistry and toxicology behind chemical fertilizers. In F. B. Lewu, T. Volova, S. Thomas, and K. R. Rakhimol (Eds.). *Controlled Release Fertilizers for Sustainable Agriculture, Academic Press*, 195–229.

4. Klimczyk, M., Siczek, A. and Schimmelpfennig, L. (2021) Improving the efficiency of urea-based fertilization leading to reduction in ammonia emission. *Science of the Total Environment*, **771**, 145483.

5. Daneshfar, A., Matsuura, T., Emadzadeh, D., Pahlevani, Z. and Ismail, A. F. (2015) Urease-carrying electrospun polyacrylonitrile mat for urea hydrolysis. *Reactive and Functional Polymers*, **87**, 37–45.

6. Russell, A. J., Erbeldinger, M., DeFrank, J. J., Kaar, J. and Drevon, G. (2002) Catalytic buffers enable positive-response inhibition-based sensing of nerve agents. *Biotechnology and Bioengineering*, **77**, 352–357.

7. Lee, Y. J., Im, E. C., Lee, G. Y. S., Hong, S. C., Lee, C. G. and Park, S. J. (2024) Comparison of ammonia volatilization in paddy and field soils fertilized with urea and ammonium sulfate during rice, potato, and Chinese cabbage cultivation. *Atmospheric Pollution Research*, **15**, 102049.

8. Wang, Y., Yao, Z. S., Wang, Y. Q., Yan, G. X., Janz, B., Wang, X. G., Zhan, Y., Wang, R., Zheng, X. H., Zhou, M. H., Zhu, B., Kiese, R., Wolf, B. and Butterbach-Bahl, K. (2023) Characteristics of annual NH_3 emissions from a conventional vegetable field under various nitrogen management strategies. *Journal of Environmental Management*, **342**, 118276.

9. Skorupka, M. and Nosalewicz, A. (2021) Ammonia volatilization from fertilizer urea-A new challenge for agriculture and industry in view of growing global demand for food and energy crops. *Agriculture*, **11**, 822.

10. Brito, T. O., Souza, A. X., Mota, Y. C. C., Morais, V. S. S., de Souza, L. T., de Fátima, Â., Macedo, F. and Modolo, L. V. (2015) Design, syntheses and evaluation of benzoylthioureas as urease inhibitors of agricultural interest. *RSC Advances*, **5**, 44507–44515.

11. Matczuk, D. and Siczek, A. (2021) Effectiveness of the use of urease inhibitors in agriculture: A review. *International Agrophysics*, **35**, 197–208.

12. Lana, R. M. Q., Pereira, V. J., Leite, C. N., Teixeira, G. M., Gomes, J. S., and Camargo, R. (2018) NBPT (urease inhibitor) in the dynamics of ammonia volatilization. *Revista Brasileira de Ciências Agrárias - Brazilian Journal of Agricultural Sciences*, **13**, e5538.

13. Al-Rooqi, M. M., Mughal, E. U., Raja, Q. A., Hussein, E. M., Naeem, N., Sadiq, A., Asghar, B. H., Moussa, Z. and Ahmed, S. A. (2023) Flavonoids and related privileged scaffolds as potential urease inhibitors: a review. *RSC Advances*, **13**, 3210–3233.

14. Liu, H., Wang, Y., Lv, M., Luo, Y., Liu, B. M., Huang, Y., Wang, M. and Wang, J. (2020) Flavonoid analogues as urease inhibitors: Synthesis, biological evaluation, molecular docking studies and in-silico ADME evaluation. *Bioorganic Chemistry*, **105**, 104370.

15. Sharaf, M., Arif, M., Hamouda, H. I., Khan, S., Abdalla, M., Shabana, S., Rozan, H. E., Khan, T. U., Chi, Z., and Liu, C. (2022) Preparation, urease inhibition mechanisms, and anti-*Helicobacter pylori* activities of hesperetin-7-rhamnoglucoside. *Current Research in Microbial Sciences*, **3**, 100103.

16. de Souza Farias, S. A., da Costa, K. S. and Martins, J. B. L. (2023) Comparative analysis of the reactivity of anthocyanidins, leucoanthocyanidins, and flavonols using a quantum chemistry approach. *Journal of Molecular Modeling*, **29**, 93.

17. Xiao, Z. P., Peng, Z. Y., Dong, J. J., He, J., Ouyang, H., Feng, Y. T., Lu, C. L., Lin, W. Q., Wang, J. X. and Xiang, Y. P. (2013) Synthesis, structure–activity relationship analysis and kinetics study of reductive derivatives of flavonoids as *Helicobacter pylori* urease inhibitors. *European Journal of Medicinal Chemistry*, **63**, 685–695.

18. Bannwarth, C., Ehlert, S. and Grimme, S. (2019) GFN2-xTB-An accurate and broadly parametrized self-consistent tight-binding quantum chemical method with multipole electrostatics and density-dependent dispersion contributions. *Journal of Chemical Theory and Computation*, **15**, 1652–1671.

19. Grimme, S., Bannwarth, C. and Shushkov, P. (2017) A robust and accurate tight-binding quantum chemical method for structures, vibrational frequencies, and noncovalent interactions of large molecular systems parametrized for all spd-block elements (Z = 1–86). *Journal of Chemical Theory and Computation*, **13**, 1989–2009.

20. Krajewska, B. (2009) Ureases I. Functional, catalytic and kinetic properties: A review. *Journal of Molecular Catalysis B: Enzymatic*, **59**, 9–21.

21. Berman, H. M., Westbrook, J., Feng, Z., Gilliland, G., Bhat, T. N., Weissig, H., Shindyalov, I. N. and

Bourne, P. E. (2000) The protein data bank. *Nucleic Acids Research*, **28**, 235–242.

22. Balasubramanian, A. and Ponnuraj, K. (2010) Crystal structure of the first plant urease from jack bean: 83 years of journey from its first crystal to molecular structure. *Journal of Molecular Biology*, **400**, 274–283.

23. Carlsson, H. and Nordlander, E. (2010) Computational modeling of the mechanism of urease. *Bioinorganic Chemistry and Applications*, **2010**, 364891.

24. Mazzei, L., Cianci, M., Contaldo, U., Musiani, F. and Ciurli, S. (2017) Urease inhibition in the presence of N-(n-Butyl)thiophosphoric triamide, a suicide substrate: Structure and Kinetics. *Biochemistry*, **56**, 5391–5404.

25. Lu, T. and Chen, F. (2012) Multiwfn: A multi-functional wavefunction analyzer. *Journal of Computational Chemistry*, **33**, 580–592.

26. Lu, T. and Manzetti, S. (2014) Wavefunction and reactivity study of benzo[a]pyrene diol epoxide and its enantiomeric forms. *Structural Chemistry*, **25**, 1521–1533.

27. Bianchi, R., Gervasio, G. and Marabello, D. (2005) The experimental charge density in transition metal compounds. *Comptes Rendus Chimie*, **8**, 1392–1399.

28. Emamian, S., Lu, T., Kruse, H. and Emamian, H. (2019) Exploring nature and predicting strength of hydrogen bonds: A correlation analysis between atoms-in-molecules descriptors, binding energies, and energy components of symmetry-adapted perturbation theory. *Journal of Computational Chemistry*, **40**, 2868–2881.

29. Kumar, S. and Pandey, A. K. (2013) Chemistry and biological activities of flavonoids: An overview. *Scientific World Journal*, **2013**, 162750.

30. Tang, H., Huang, L., Sun, C. and Zhao, D. (2020) Exploring the structure–activity relationship and interaction mechanism of flavonoids and α-glucosidase based on experimental analysis and molecular docking studies. *Food & Function*, **11**, 3332–3350.

31. Zhao, J., Huang, L., Sun, C., Zhao, D. and Tang, H. (2020) Studies on the structure-activity relationship and interaction mechanism of flavonoids and xanthine oxidase through enzyme kinetics, spectroscopy methods and molecular simulations. *Food Chemistry*, **323**, 126807.

32. Cramer, J., Sager, C. P. and Ernst, B. (2019) Hydroxyl groups in synthetic and natural-product-derived therapeutics: A perspective on a common functional group. *Journal of Medicinal Chemistry*, **62**, 8915–8930.

33. Aparicio, S. (2010) A systematic computational study on flavonoids. *International Journal of Molecular Sciences*, **11**, 2017–2038.

34. Trott, O. and Olson, A. J. (2010) AutoDock Vina: Improving the speed and accuracy of docking with a new scoring function, efficient optimization, and multithreading. *Journal of Computational Chemistry*, **31**, 455–461.

35. Estiu, G. and Merz, K. M. (2007) Competitive hydrolytic and elimination mechanisms in the urease catalyzed decomposition of urea. *The Journal of Physical Chemistry B*, **111**, 10263–10274.

36. Jabri, E., Carr, M. B., Hausinger, R. P. and Karplus, P. A. (1995) The crystal structure of urease from klebsiella aerogenes. *Science*, **268**, 998–1004.

37. Ullah, S., Halim, S. A., Ibrar, A., Khan, I., Ataya, F. S., Fouad, D., Batiha, G. E. -S., Khan, A. and Al-Harrasi, A. (2023) Urease inhibitory potential of pyridine-containing triazolothiadiazole and triazolothiadiazine scaffolds for the treatment of ulceration and kidney stone: in vitro screening, kinetics mechanism, and in silico computational analysis. *Journal of Biomolecular Structure and Dynamics*, 1–10.

38. Aman, H., Rashid, N., Ashraf, Z., Bibi, A., Chen, H. -T. and Sathishkumar, N. (2020) Synthesis, density functional theory (DFT) studies and urease inhibition activity of chiral benzimidazoles. *Heliyon*, **6**, 1-8e05187.

39. Rizwana, F. B., Prasana, J. C., Muthu, S. and Abraham, C. S. (2019) Molecular docking studies, charge transfer excitation and wave function analyses (ESP, ELF, LOL) on valacyclovir : A potential antiviral drug. *Computational Biology and Chemistry*, **78**, 9–17.

40. Espinosa, E., Alkorta, I., Elguero, J. and Molins, E. (2002) From weak to strong interactions: A comprehensive analysis of the topological and energetic properties of the electron density distribution involving X–H···F–Y systems. *The Journal of Chemical Physics*, **117**, 5529–5542.

41. Awllia, J. A. J., Al-Ghamdi, M., Huwait, E., Javaid, S., Atia tul, W., Rasheed, S. and Choudhary, M. I. (2016) Flavonoids as natural inhibitors of jack bean urease enzyme. *Letters in Drug Design & Discovery*, **13**, 243–249.

42. Kataria, R. and Khatkar, A. (2019) Lead molecules for targeted urease inhibition: An updated review from 2010-2018. *Current Protein and Peptide Science*, **20**, 1158–1188.